

Deletion of the Complex I Subunit *NDUFS4* Adversely Modulates Cellular Differentiation

Jacqueline Johnson,^{1,2,*} William Lee,^{1,2,*} Ann E. Frazier,^{3,4} Vijesh Vaghjiani,^{1,2}
Adrienne Laskowski,³ Alexandra L. Rodriguez,⁵ Gael L. Cagnone,^{1,2} Matthew McKenzie,^{1,2}
Stefan J. White,^{1,2} David R. Nisbet,⁵ David R. Thorburn,^{3,4} and Justin C. St. John^{1,2}

The vast majority of cellular ATP is produced by the oxidative phosphorylation (OXPHOS) system, which comprises the four complexes of the electron transfer chain plus the ATP synthase. Complex I is the largest of the OXPHOS complexes, and mutation of the genes encoding either the subunits or assembly factors of Complex I can result in Complex I deficiency, which is the most common OXPHOS disorder. Mutations in the Complex I gene *NDUFS4* lead to Leigh syndrome, which is the most frequent presentation of Complex I deficiency in children presenting with progressive encephalopathy shortly after birth. Symptoms include motor and intellectual retardation, often accompanied by dystonia, ataxia, and growth retardation, and most patients die by 3 years of age. To understand the origins of this disease, we have generated a series of mouse embryonic stem cell lines from blastocysts that were wild type, heterozygous, and homozygous for the deletion of the *Ndufs4* gene. We have demonstrated their pluripotency and potential to differentiate into all cell types of the body. Although the loss of *Ndufs4* did not affect the stability of the mitochondrial and nuclear genomes, there were significant differences in patterns of chromosomal gene expression following both spontaneous differentiation and directed neural differentiation into astrocytes. The defect also affected the potential of the cells to generate beating embryoid bodies. These outcomes demonstrate that defects associated with Complex I deficiency affect early gene expression patterns, which escalate during early and later stages of differentiation and are mediated by the defect and not other chromosomal or mitochondrial DNA defects.

Introduction

THE VAST MAJORITY OF CELLULAR ATP is produced by the biochemical process of oxidative phosphorylation (OXPHOS) [1]. The OXPHOS system, which is located in the mitochondrion, consists of five protein complexes (I–V) that each comprises multiple subunits encoded by the nuclear and mitochondrial DNA (mtDNA) genomes [2,3]. Disorders associated with OXPHOS are the most common group of inborn errors of metabolism, affecting ~1:5,000 births [4]. While all tissues or organs of the body can be affected, tissues and organs with a high requirement for energy, such as the brain, heart, and muscle, are most at risk [3,5]. Many patients presenting with OXPHOS disorders display neurological symptoms that are often episodic and become progressive leading to premature death [6].

Complex I is the largest of the OXPHOS complexes comprising 44 subunits, 7 of which are encoded by mtDNA. Its assembly requires a number of assembly factors, which are

encoded by the nuclear genome [7,8]. Mutation of the genes encoding either the subunits or assembly factors of Complex I can result in Complex I deficiency, which is the most common OXPHOS disorder [9,10]. *NDUFS4* is a nuclear gene that encodes a matrix arm subunit of Complex I. Mutations in *NDUFS4* lead to assembly/stability defects and a severe defect in Complex I activity [11]. Patients with mutations in the *NDUFS4* gene typically develop Leigh syndrome [12,13]. Leigh syndrome is the most frequent presentation of Complex I deficiency in children and typically presents a few months after birth with progressive encephalopathy [14]. Symptoms include motor and intellectual retardation, frequently accompanied by dystonia, ataxia, and growth retardation, with most patients dying by 3 years of age [14,15]. Comparable defects in Complex I activity and assembly have been observed in *Ndufs4*^{-/-} mice, which develop neurological symptoms from week 5 onward leading to death at 7 weeks [11,16].

Much of our understanding of the pathogenesis of OXPHOS defects is derived from studies using patient

¹Centre for Genetic Diseases, Hudson Institute of Medical Research, Clayton, Australia.

²Department of Molecular and Translational Science, Monash University, Clayton, Australia.

³Murdoch Childrens Research Institute, Royal Children's Hospital, Melbourne, Australia.

⁴Department of Pediatrics, University of Melbourne, Melbourne, Australia.

⁵Research School of Engineering, Australian National University, Canberra, Australia.

*These authors contributed equally to this work.

fibroblasts. Although informative, this cell type does not reflect the tissues contributing to the phenotypes observed in mitochondrial disease as they do not require high ATP generation. Several Complex I-deficient mouse models have now been described, which provide access to tissues, such as the brain [11,17,18]. However, analyses of these models are usually restricted to postmitotic tissues. With mutations in more than 100 genes implicated in mitochondrial disease, it is essential to establish the contribution of mutations in specific genes to disease pathogenesis in a cell-specific manner and during development [19].

Embryonic stem (ES) cells are derived from the inner cell mass (ICM) of the blastocyst stage embryo [20]. They have the potential to self-renew and are pluripotent as they can differentiate into all cell types of the body. During differentiation, they first give rise to progenitor and multipotent stem cells, which are precursors that then commit to lineage-specific mature cell types. Consequently, ES cells are important for the study of pluripotency, differentiation, development, epigenetic regulation, and lineage-specific gene expression [21]. In this respect, they enable studies to be performed at various stages to determine when a specific genetic defect first affects differentiation and whether there are lineage-specific biases that would account for the phenotypes observed. Furthermore, they are excellent models to test the effects of metabolic defects on development as self-renewing cells rely extensively on anaerobic glycolysis to promote their quiescent state and then switch to mitochondrial OXPHOS as differentiation takes place [22]. High ATP-requiring mature cells will then use OXPHOS to meet their functional demands [23]. For example, neural cells will require extensive levels of OXPHOS-derived ATP to promote trafficking of transmitters, while spleen and sperm cells have very low requirements for OXPHOS-derived ATP and primarily use glycolysis. This can be mediated by cells regulating their levels of mtDNA copy number during development [24–26], but mutation or deletion to any of the coding genes of the electron transfer chain (ETC) would likely hinder the process of differentiation.

As many of the Complex I-deficient syndromes affect children and are thus likely to have their origins in early development, we have generated a series of mouse ES cell lines from blastocysts that were wild type, heterozygous, and homozygous for the deletion of the *Ndufs4* gene of Complex I. This Complex I-deficient mouse model arose through spontaneous B2 SINE retroviral insertion into the *Ndufs4* gene [11]. While the defect exerted little pressure on the stability of the mitochondrial and nuclear genomes, it was evident that there were differences in patterns of chromosomal gene expression following both spontaneous differentiation and directed differentiation into astrocytes. These outcomes demonstrate that mutations associated with Complex I deficiency affect early gene expression patterns that have a compounding effect later during differentiation.

Materials and Methods

Derivation of ES cell lines

Ndufs4^{+/*fky*} mice [11] were crossed for 10 generations to BALB/c mice to generate the congenic mice used for embryo collection. Experimental procedures were performed according to an approved ethics protocol granted by the

Murdoch Childrens Research Institute Animal Ethics Committee (A662). Male *Ndufs4*^{+/*fky*} (+/–) mice were mated with 60-day-old female *Ndufs4*^{+/*fky*} mice superovulated with 5 IU/mouse Folligon and Chorulon according to Nagy et al. [27]. Day 2.5 embryos were flushed from dissected oviducts and embryos collected in M2 media (M7167; Sigma), transferred to KSOM media (MR020P5F; Merck Millipore), and cultured at 37°C in 5% CO₂. Embryos were monitored to check for development to the blastocyst stage. Expanded blastocysts were transferred singly to mouse embryonic fibroblast (MEF) feeder plates and cultured in mouse ES cell media supplemented with 5,000 U mouse leukemia inhibitory factor (LIF; ESG1107; Merck Millipore), as previously described by Kelly et al. [26], for 4–5 days, with media change on day 3. Hatched blastocysts attached to the feeder layer with the ICM forming a small mound of cells in the middle of an outgrowth of trophoblasts. After 4–5 days, under a dissecting microscope (Leica MZ6), ICMs were picked, dissociated with TrypLE (12604021; Life Technologies), individually replated onto fresh feeder plates, and cultured as before, with media change every 2–3 days. Following a further 6–7 days of culture, putative ES cell colonies were visible in some of the dissociated ICM plates. Individual colonies were picked, dissociated, and subcultured using the same method as for ICMs. Four to five days later, colonies were dissociated with TrypLE and passaged to larger wells for expansion. Putative ES colonies were passaged and expanded every 3–4 days, and stocks were frozen at early passage. The established cell lines are referred to as wild-type (+/+), heterozygous (+/–), and homozygous null (–/–) cell lines.

Genotyping

ES cells were genotyped using standard polymerase chain reaction (PCR) conditions with one forward primer in intron 3 of the *Ndufs4* gene (5'-TAGGAAGGGAGACGAGCA-3') and two reverse primers. One was located in the B2 SINE insert (5'-TTACCCACTGAGCCATCTCAC-3') and the other in exon 3 (5'-GATGCCCAACCCATCAAAG-3'), as described by Leong et al. [11].

Agilent microarray hybridization and analysis

Genomic DNA was isolated from each sample using the QIAGEN DNeasy Blood and Tissue Kit (69504). DNA labeling was performed according to the Agilent protocol, with the test samples labeled with Cy5 and the reference samples labeled with Cy3. Each labeled test sample was combined with a labeled reference sample and hybridized onto an Agilent 4x180K mouse CGH microarray (no. G4839A). Microarray washing, scanning, and data extraction were performed, according to the manufacturer's instructions. Data were analyzed using Agilent Workbench 7.0, and the ADM-2 algorithm was used with default settings. A threshold of four consecutive probes was used when calling a copy number variant (CNV).

Assessment of mtDNA copy number

Total DNA was extracted using the QIAGEN DNeasy Blood and Tissue Kit (69504), according to the manufacturer's instructions. The samples were then treated with RNase solution (19101; QIAGEN) for 5 min at 37°C to

obtain RNA-free DNA. Reactions were performed in a RotorGene 3000 real-time PCR machine (Corbett Research), as previously described [19], using primers listed in Supplementary Table S1 (Supplementary Data are available online at www.liebertpub.com/scd).

Blue native polyacrylamide gel electrophoresis and spectrophotometric enzyme assays

Blue native polyacrylamide gel electrophoresis (BN-PAGE) was performed, as previously described [28]. In brief, ~50 µg of whole cells were solubilized in 1% (v/v) Triton X-100 and resolved on a 4%–13% blue native gradient gel. Native protein complexes were transferred to PVDF membrane for western blotting and probed with antibodies against the Complex I subunit NDUFA9 and the Complex II subunit SDHA (MitoSciences). Spectrophotometric enzyme assays for Complex I (rotenone-sensitive NADH-CoQ₁ oxidoreductase) and the mitochondrial marker enzyme citrate synthase were performed on post-600g supernatants from cultured ES cells and their derivatives (~10⁷ cells per line), as described previously [29]. Complex I activity is expressed relative to citrate synthase to allow for any differences in mitochondrial content between cell cultures.

Next-generation sequencing of the mitochondrial genome

Two overlapping fragments that each spans half of the mitochondrial genome were generated by long PCR amplification as templates for next-generation sequencing, which was performed and analyzed as described by Sobinoff et al. and Yeung et al. [30,31] and detailed in Supplementary Data.

Analysis of FGF-21 release in cell media via enzyme-linked immunosorbent assay

After 3 days of culture, cell media from each experimental group were analyzed for FGF-21 release using a solid-phase sandwich enzyme-linked immunosorbent assay (ELISA) kit (Quantikine ELISA: Mouse/Rat FGF-21; R&D Systems). The media were centrifuged to remove any particulates, and the supernatant was tested for FGF-21. The ELISA was carried out as per the manufacturer's instructions, and all samples were analyzed in triplicate. Absorbance was measured using an Infinite 200Pro plate reader (Tecan) at a wavelength of 450 nm.

Measurements of O₂ consumption rates

O₂ consumption rates were determined by high-resolution respirometry with an oxygraph (Oxygraph-2K; Oroboros), according to the manufacturer's instructions. Five millimolars of malate and 5 mM glutamate were added into chambers containing 2 mL respiration buffer (225 mM mannitol, 75 mM sucrose, 10 mM KCl, 10 mM Tris-HCl, and 5 mM KH₂PO₄, pH 7.2). Mitochondria were isolated from cells, as described previously [32]. One milligram of isolated mitochondria was transferred into chambers containing respiration buffer; malate and glutamate maintained at 30°C and continuously stirred at 750 rpm. O₂ consumption was measured using the integrated software package DatLab (version 3.1; Oroboros), which presented respiration as pmol O₂ flux per mg per second. Initial resting measurements (state IV) were recorded for 5 min, after

which 187.5 µM ADP (Sigma-Aldrich) was added to the chambers to measure state III respiration for 15 min.

ATP quantification and cellular lactate production

ATP content and lactate production were quantified using the ATPlite Assay Kit (6016943; PerkinElmer) and Lactate Assay Kit II (K627-100; BioVision), respectively, according to the manufacturer's conditions, as described by Kelly et al. [19].

Immunocytochemistry

For immunocytochemical analysis, cells were fixed, permeabilized, and nonspecific binding sites blocked, as described by Dickinson et al. [33]. Primary antibodies used for undifferentiated cells were OCT4 (sc5279; Santa Cruz) and SSEA1 (MAB4301; Merck Millipore) (both 1:50) and SOX2 (ab69893; Abcam) and NANOG (145761; eBioscience) (both 1:100). For differentiated cells, primary antibodies for NESTIN (MAB353; Merck Millipore) and βIII-tubulin (ab18207; Abcam) (both 1:500) and MAP2 (AB5622; Merck Millipore), GFAP (MAB360; Merck Millipore), smooth muscle actin (CBL171; Merck Millipore), and alpha-fetoprotein (MAB1368; R&D Systems) (all 1:200) were used. All primary antibodies were incubated for 2 h at room temperature, and all secondary antibodies (AlexaFluor, 1:500; Life Technologies) were incubated for 1 h at room temperature in the dark. ProLong Gold Antifade with DAPI (P36931; Life Technologies) was used as a nuclear stain and mountant, as per the manufacturer's instructions. Immunofluorescent staining was visualized on an Olympus IX70 microscope.

Teratoma formation

1 × 10⁶ cells were injected into the testis capsule of 4- to 6-week-old severe combined immunodeficient (SCID) mice by approved Monash Animal Research Platform staff following their standard operating procedure (SOP0159). Teratomas were excised between 4 and 8 weeks and fixed in Bouin's Fluid (Amber Scientific). The fixed tissue was processed at the Hudson Institute of Medical Research Histology Core Facility using standard methods for paraffin embedding, sectioning at 4 µm, and hematoxylin and eosin staining.

Spontaneous differentiation of ES cell lines

ES cells were induced to form embryoid bodies (EBs) by aliquoting a suspension of 5 × 10³ cells/mL in ES cell, no LIF, media to low attachment plates. EBs were cultured in suspension for 7 days and then transferred to 0.1% gelatin-coated tissue culture plates to allow attachment and spontaneous differentiation to occur. ES cell, no LIF, media were changed every 3–4 days, and cells were differentiated up to 25 days. To assess the potential of ES cells to differentiate into beating cardiomyocytes, single EBs were plated to each well of a 0.1% gelatin-coated, 24-well plate and cultured for 21 days, with observations recorded every 2 days.

Directed differentiation of ES cell lines into neural lineages

Undifferentiated ES cells were dissociated and plated onto 0.1% gelatin-coated tissue culture plates at a density of 1.5–2 × 10⁴/cm² in ES cell, no LIF, media. After 2 days,

media were changed to N2B27 medium, composed of Dulbecco's modified Eagle medium/nutrient mixture F-12 (DMEM/F12; 10565018; Life Technologies) supplemented with 2% B27 (17504044; Life Technologies), 1% N2 (17502048; Life Technologies), and 10 ng/mL bFGF (GF003; Merck Millipore). Media were renewed every 2 days. At day 7, the cultures were dissociated using Accutase (A6964; Sigma) and plated at 5×10^4 cells/cm² and cultured further on a fibronectin substrate in DMEM/F12 media with 1% N2 and 2% fetal bovine serum (10099141; Life Technologies) for differentiation into astrocytes.

RT² PCR array analysis

Total RNA was extracted from ES cells using the RNeasy Kit (74104; QIAGEN), according to the manufacturer's protocol. Complementary DNA (cDNA) was synthesized using the RT² First Strand Kit (330401; SABiosciences) [33]. Undifferentiated and spontaneously differentiated (days 7 and 25) ES cells were analyzed using the Mouse Cell Lineage Identification RT² ProfilerTM PCR Array (PAMM508Z; SABiosciences). Neural directed differentiated cells from day 7 were analyzed using the Mouse Neurogenesis RT² Profiler PCR Array (PAMM404Z; SABiosciences). Each cell line was differentiated in triplicate to create biological triplicates. Reactions were performed in triplicate for each biological replicate in 384-well optical reaction plates (SABiosciences), as described by Dickinson et al. [33]. Analysis was performed using the Web-Based PCR Array Data Analysis Software (SABiosciences), as described by Dickinson et al. [33].

Gene expression analysis by real-time reverse transcription-PCR (RT-PCR)

RNA extraction was performed, as previously described by Kelly et al. [19], and then reverse transcribed with SuperScript III (18080044; Life Technologies), according to the manufacturer's instructions. Reactions were performed in a RotorGene 3000 real-time PCR machine (Corbett Research), as described by Kelly et al. [19], using primers listed in Supplementary Table S1. Each cell line was cultured and differentiated in triplicate to create biological triplicates. For each time point, each replicate was then assayed in triplicate.

Statistical analyses

Statistical analyses were performed using GraphPad Prism 5.01 (GraphPad Software, Inc.). Data are expressed as mean \pm standard error of the mean. Bartlett's test for equal variances was used to determine whether the data were distributed normally. Significant differences in gene expression were determined using one-way or two-way ANOVA and Bonferroni post-hoc tests.

Results

Derivation of ES cell lines

Embryos were retrieved from female *Ndufs4*^{+/*fky*} mice 2 days after insemination by male *Ndufs4*^{+/*fky*} mice and allowed to develop in culture to the blastocyst stage. From 60 embryos harvested, 51 developed to the blastocyst stage, resulting in the generation of 4 fully characterized ES cell lines (Supplementary Table S2). This represents an overall ES cell derivation rate of 7.84%.

Genotyping of the ES cell lines

We genotyped each of the lines by PCR and demonstrated that two of the lines were wild type (+/+), one was heterozygous (+/-), and one was homozygous null (-/-) (Fig. 1A). Genotyping of the ES cell lines was supported by BN-PAGE blotting, which demonstrated that Complex I was present in the wild-type and heterozygous ES lines. However, an intermediate of \sim 800 kDa was present in the homozygous null (Fig. 1B), which is indicative of an *NDUFS4* defect.

We also assessed each of the lines for CNVs. Only one line, namely wild-type line #1, showed evidence of a CNV, a 107-kb duplication on chromosome 9 (chr9:112194351–112301758, mm9) at passage 3. As mtDNA copy number is strictly regulated in pluripotent cells, we assessed mtDNA copy number in undifferentiated cells. There were significant differences between each of the lines, although each of the lines possessed between 554 ± 9 and 746 ± 19 copies of mtDNA (Fig. 1C).

We further performed mtDNA next-generation sequencing on each of the lines at early and late stage passage to determine whether deletion of *Ndufs4* exerted pressure on the integrity of the mitochondrial genome. In all, 22 variants were identified in the four lines, of which 4 were single-nucleotide, nonsynonymous variants at nt 4289, 4299, and 4889 (all *Nd2*) and 15166 (*CytB*) (Supplementary Table S3). Likewise, the insertion at nt 10502 (*Nd4*) was also nonsynonymous. The most frequently observed nonsynonymous variant was at nt 4289. It was either lost or gained in the wild-type and heterozygous early and late passage cells but persisted in the homozygous null cells. It was also present at the highest level (range = 12.49%–16.97%). However, the most persistent variant was an insertion at nt 1636 in the *rRNA2* (*16S rRNA*) gene. Only the variant at 15166 was specific to the homozygous null cells.

O₂ consumption, total cellular ATP and lactate levels, Complex I activity, and FGF-21

We measured O₂ consumption rates, ATP content, and lactate production in each of the lines. There were significant differences in O₂ consumption rates for isolated mitochondrial populations between the wild-type and heterozygous cells and the homozygous null cells (Fig. 1D, $P < 0.05$; Supplementary Table S4). However, there were no significant differences in ATP content and lactate production between the cell lines (Supplementary Table S4). Spectrophotometric enzyme assays showed lower activity of Complex I in homozygous null cells than in wild-type and heterozygous cells (Table 1).

In addition, as it has been previously reported that *FGF-21* is a marker of mitochondrial disease [34], we assessed culture media from each of the lines for levels of *FGF-21* using an ELISA assay. There were significant differences between each of the wild-type and heterozygous and homozygous null cell lines, with higher levels in the heterozygous and homozygous null cell lines (Fig. 1E).

Characterization of the ES cell lines

Each of the lines was assessed for its pluripotent potential. First, we determined whether they expressed the key markers of the pluripotent network comprising OCT4, SOX2, and

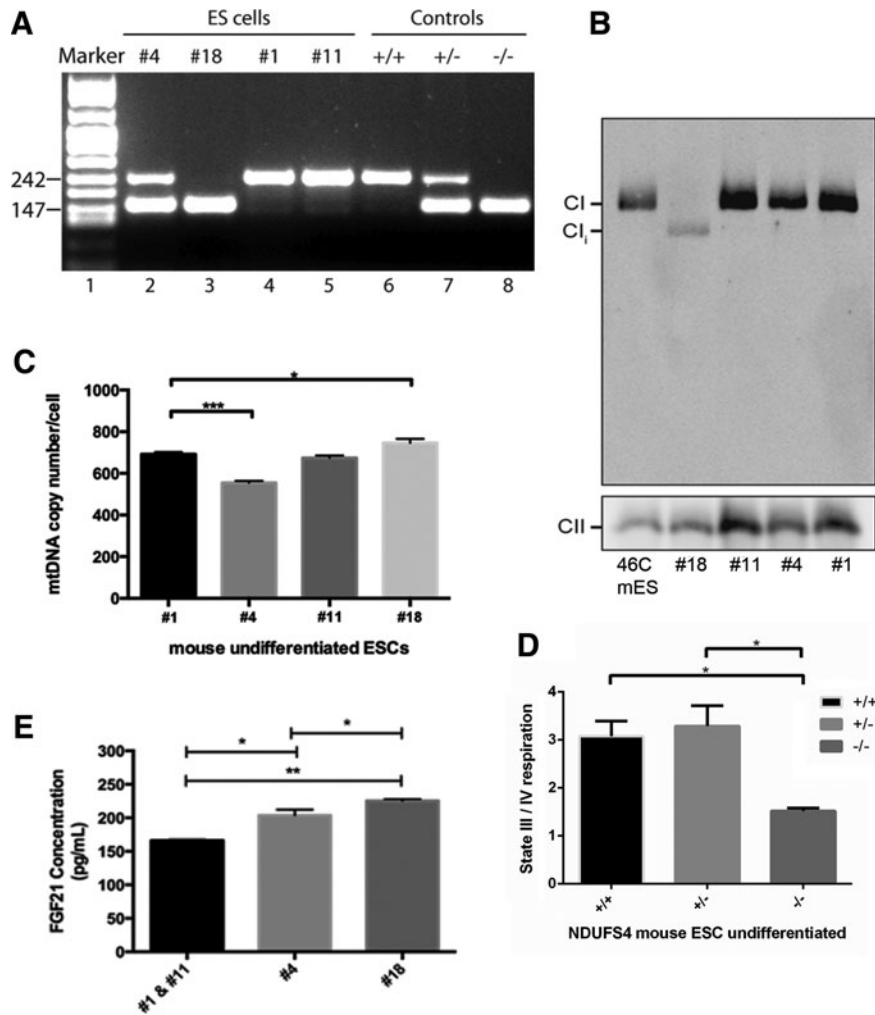


FIG. 1. Genotyping of ES cells. **(A)** Polymerase chain reactions were performed using genomic DNA prepared from ES cell pellets (lanes 2–5; #1, #4, #11, and #18), as well as from mouse tissue lysates (controls; lanes 6–8; +/+, +/-, and +/+), to distinguish between wild-type (*Ndufs4*^{+/+}), heterozygous (*Ndufs4*^{+/-}), and knockout (*Ndufs4*^{-/-}) genotypes. Size markers (bp) are indicated. **(B)** BN-PAGE and immunodetection of Complex I in *Ndufs4* ES cell lines. ES cells were solubilized in 1% (v/v) Triton X-100 and resolved by BN-PAGE for immunodetection. Mature Complex I (~980 kDa) is visible in the control ES cell line (46C mES) and ES lines #11, #4, and #1. An incompletely assembled form of Complex I (~800 kDa, CI_i) was detected in ES line #18. This complex corresponds to the crippled Complex I that is associated with mutant *Ndufs4* [11] and verifies the loss of *NDUFS4* in this line. Complex II (CII) is shown as a loading control. **(C)** MtDNA copy number (mean ± SEM) for wild-type (#1 and #11), heterozygous (#4), and homozygous null (#18) undifferentiated ES cells. **(D)** O₂ consumption rates assayed on isolated mitochondria for wild-type (+/+), heterozygous (+/-), and homozygous null (-/-) undifferentiated ES cells, expressed as the ratio of state III (ADP linked) to state IV (basal) rate. **(E)** Levels of FGF-21 (mean ± SEM) for wild-type (#1 and #11), heterozygous (#4), and homozygous null (#18) undifferentiated ES cells. #1 and #11 = +/+; #4 = +/-; #18 = -/-. **P* < 0.05; ***P* < 0.01; ****P* < 0.001. BN-PAGE, blue native polyacrylamide gel electrophoresis; ES, embryonic stem; mtDNA, mitochondrial DNA; SEM, standard error of the mean.

TABLE 1. COMPLEX I ACTIVITY IN UNDIFFERENTIATED EMBRYONIC STEM CELLS AND CELLS FOLLOWING SPONTANEOUS DIFFERENTIATION OR DIRECTED NEUROGENESIS

	#1 (+/+)	#11 (+/+)	#4 (+/-)	#18 (-/-)
Undifferentiated embryonic stem cell	133	133	111	90
Spontaneous (day 18)	170	177	100	68
Spontaneous (day 25)	114	149	91	79
Directed neurogenesis (day 7)	122	107	123	86
Directed neurogenesis (day 14)	86	65	58	49
Directed neurogenesis (day 21)	n.d.	94	49	57

Complex I activity is expressed relative to citrate synthase to allow for any differences in mitochondrial content between cell cultures. Values are the means of duplicate estimates. Significance of differences between cell lines was determined by a paired two-tailed *t*-test comparing each set of six cell culture conditions for mean value of +/+ versus +/- (*P* < 0.05), mean value of +/+ versus -/- (*P* < 0.01), and +/- versus -/- (*P* < 0.05).

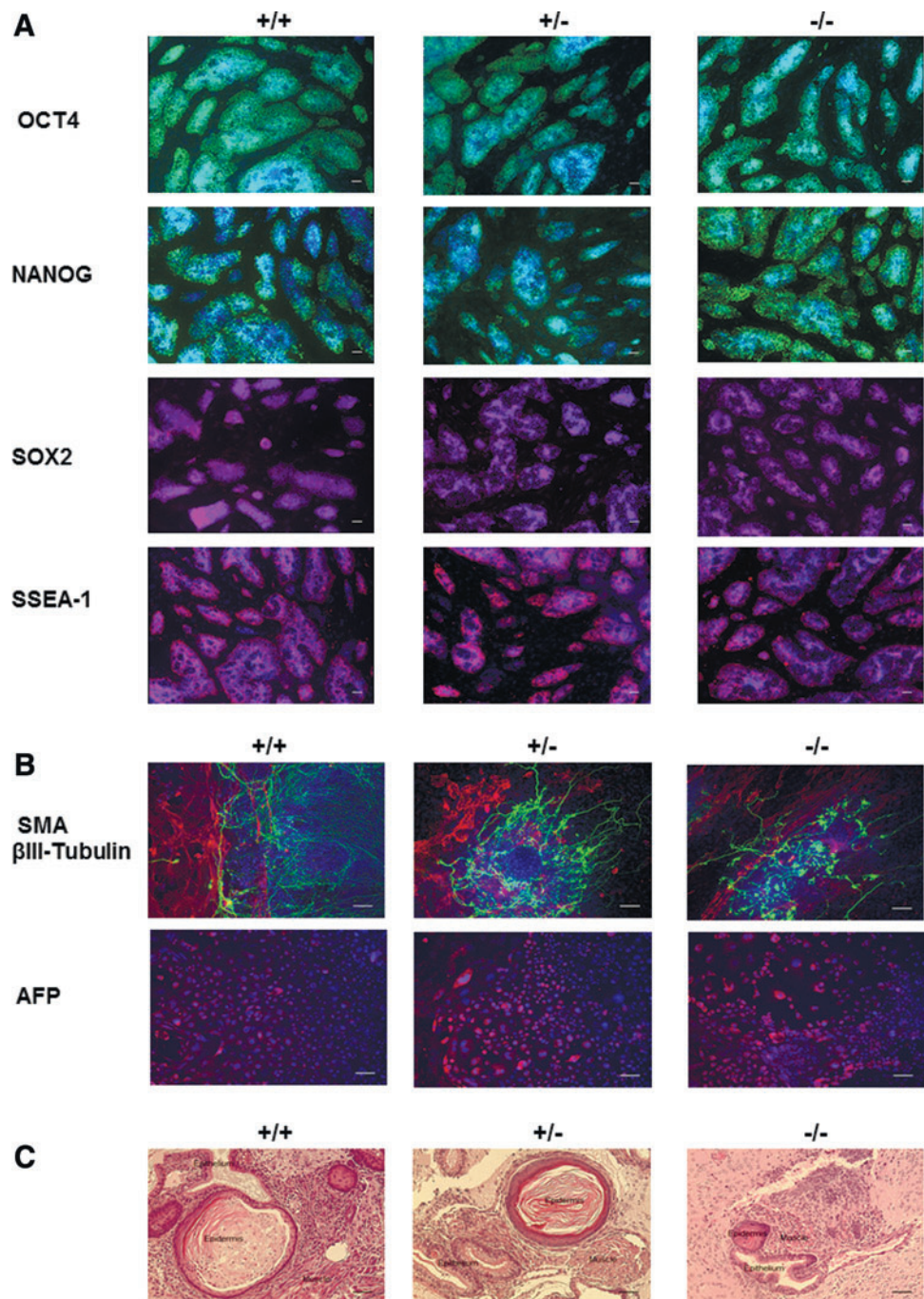
n.d., not determined.

NANOG. As can be seen from Fig. 2A and Supplementary Fig. S1, each of the lines expressed the pluripotent genes along with the cell surface marker, SSEA1, a marker of undifferentiated cells. Second, as can be seen from Fig. 2B, each of the lines has the potential to give rise to differentiated markers from each of the germ layers. We further demonstrated this by injecting cells from each of the lines into the testis capsule of SCID mice. The teratomas derived from each of the lines demonstrated the pluripotent potential through their ability to differentiate into multiple lineages. These included muscle, epithelium, and epidermis, indicative of mesoderm, endoderm, and ectoderm, respectively (Fig. 2C). These outcomes demonstrate the pluripotent potential of each of the lines.

Differentiation of the ES cell lines—early stages

As each of the lines has the ability to form teratomas and, thus, the potential to differentiate, we analyzed whether there were lineage-specific biases resulting from the degree of mutation during early and late stages of differentiation using a PCR lineage identification array. Following the induction of spontaneous differentiation, we first analyzed cells on day 7. Cluster analysis demonstrated large differences between the wild-type, heterozygous, and homozygous null lines, with the latter two clustering more closely (Fig. 3). Analysis of genes associated with pluripotency demonstrated that expression of the de novo methyltransferase *Dnmt3b* was significantly

FIG. 2. Characterization of ES cell lines. (A) Expression of pluripotent markers OCT4 (green), NANOG (green), and SOX2 (red) and the marker for undifferentiated cells, SSEA1 (red), as determined by immunocytochemistry. Nuclei were stained with DAPI (blue). Scale bar = 50 μ m; magnification = 10 \times . (B) Immunocytochemistry, at day 18, of cells generated from embryoid bodies confirmed expression of differentiation markers for mesoderm, SMA (red); endoderm, AFP (red); and ectoderm, β III-tub (green). Nuclei were stained with DAPI (blue). Scale bar = 50 μ m; magnification = 20 \times . (C) Hematoxylin and eosin staining shows that teratomas from each cell line contained multiple tissues, demonstrating that all three germ layers could be generated. Included were epidermis (ectoderm), muscle (mesoderm), and epithelium (endoderm). Scale bar = 50 μ m; magnification = 20 \times . β III-tub, β III-tubulin; AFP, alpha-fetoprotein; SMA, smooth muscle actin. Color images available online at www.liebertpub.com/scd



reduced in heterozygous and homozygous null cells ($P < 0.001$), with a similar tendency for levels of *Lefty 1* and *Nanog*, while *Zfp42* exhibited a tendency to elevated levels in heterozygous and homozygous null cells (Supplementary Fig. S2 and Supplementary Table S5).

It was evident that there were variable patterns of gene expression between heterozygous and homozygous null cells and wild-type cells for *FoxD3*, which is associated with the early germ layer, ectoderm (Supplementary Fig. S3A and Supplementary Table S5), and *Neurog2* in the neuroectoderm (Supplementary Fig. S3B and Supplementary Table S5). Likewise, for the early germ layer mesoderm, there were significantly lower levels of expression for *Pdgfra* in the heterozygous and homozygous null lines ($P < 0.001$; Supplementary Fig. S3C

and Supplementary Table S5) and *Dcn* in the homozygous null lines ($P < 0.05$). There were significantly higher levels of expression for *Mixl* in the heterozygous and homozygous null lines. For the early germ layer, endoderm, the patterns of expression for *FoxA1* were significantly higher in the heterozygous cells, while *Gata6* was only expressed in the wild-type cells (Supplementary Fig. S3D and Supplementary Table S5).

For the progenitor ectoderm, there was a tendency to increase gene expression in the heterozygous and homozygous null lines for *Hes5*, *Msln*, *Foxg1*, and *Olig2* and for *Slc32a1* in the heterozygous cells only (Supplementary Fig. S4A and Supplementary Table S5). For the progenitor mesoderm, the levels of expression were higher in the heterozygous and homozygous null lines for *Ptcr* and *Cd34* (Supplementary Fig. S4B and Supplementary Table S5). For the progenitor endoderm, expression of *Map3k12* was significantly higher for the heterozygous cells compared with the wild type ($P < 0.001$; Supplementary Fig. S4C and Supplementary Table S5). These outcomes demonstrate that, while each of the lines can express genes associated with each of the early lineages, there are biases in the heterozygous and homozygous null lines.

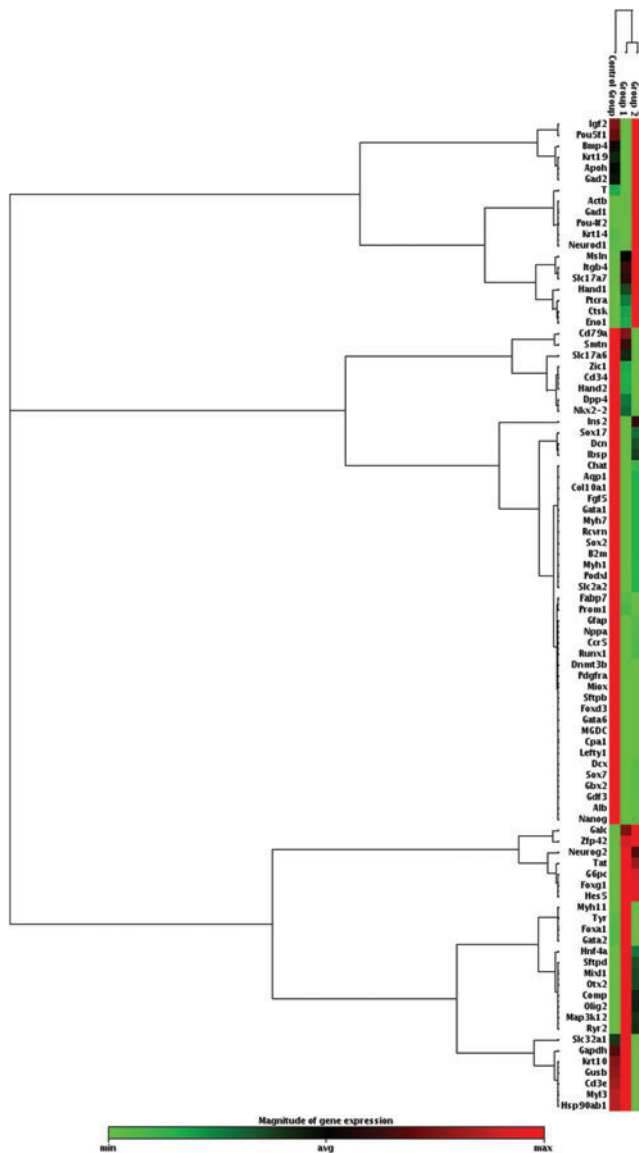


FIG. 3. Heat map of gene expression and clustering from a lineage identification array performed on day 7 differentiated ES cells. A total of 80 genes were assessed, including pluripotent, ectodermal, mesodermal, and endodermal lineages. Control is wild type, group 1 is +/-, and group 2 is -/-. Color images available online at www.liebertpub.com/scd

Differentiation of the ES cell lines—late stages

To determine whether the changes in early gene expression patterns for the heterozygous and homozygous null lines affected terminal differentiation, we analyzed cells on day 25 of spontaneous differentiation. As for the early markers, cluster analysis demonstrated that the large differences observed between the wild-type and heterozygous and homozygous null lines were maintained (Fig. 4 and Supplementary Table S6).

For the terminally differentiated markers of the ectoderm lineage, expression of *Krt14* ($P < 0.001$; Supplementary Fig. S5A and Supplementary Table S6) was lost, but there were significant increases for *Scl7a7* in both the heterozygous and homozygous null lines ($P < 0.05$) and *Gad1* in the homozygous line ($P < 0.001$). For the terminally differentiated mesoderm, levels of expression in the heterozygous and homozygous null lines were higher for *Ryr2*, while *Nppa* was significantly higher in the heterozygous line (Supplementary Fig. S5B and Supplementary Table S6). Similar patterns were observed for terminally differentiated endoderm genes, where there was a bias toward either the heterozygous line or the heterozygous and homozygous null lines, especially for *Cpa1* ($P < 0.01$; Supplementary Fig. S5C and Supplementary Table S6) and *Sfpd* ($P < 0.001$), respectively. Interestingly, for *Alb*, *Sfpb*, and *Miox*, there was no expression in the heterozygous and homozygous null lines ($P < 0.001$; Supplementary Table S6). This indicates that there are very different patterns of gene expression in the terminally differentiated cells.

Generation of beating EBs

Although there was disparity in the levels of mesodermal gene expression patterns, each of the cell lines produced beating EBs (Supplementary Table S7). The homozygous null line produced more beating EBs on days 9 and 11 of differentiation. By day 15, the numbers observed in wild-type cells were considerably higher than those in heterozygous and homozygous null lines, and this trend was

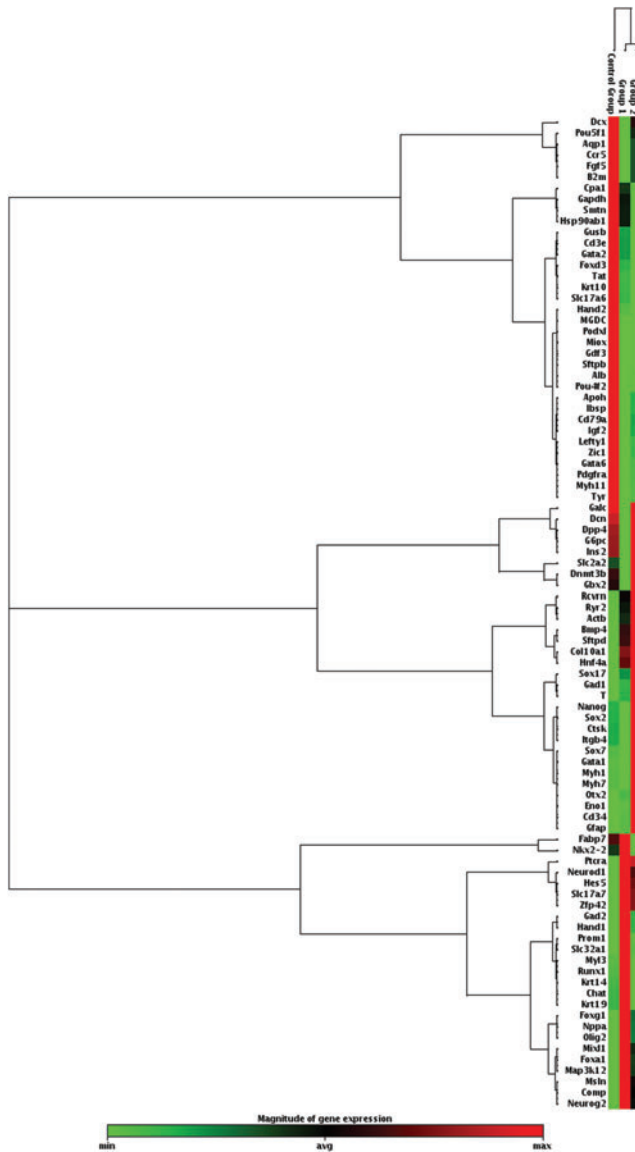


FIG. 4. Heat map of gene expression and clustering from a lineage identification array performed on day 25 differentiated ES cells. A total of 80 genes were analyzed comprising pluripotent, ectodermal, mesodermal, and endodermal lineages. Control is wild type, group 1 is +/-, and group 2 is -/-. Color images available online at www.liebertpub.com/scd

maintained through to day 21 of differentiation. Notably, the heterozygous line produced fewer beating EBs at each time point.

Directed neurogenesis

As we identified distinct biases in early and late ectodermal gene expression patterns, we performed gene expression analysis on cells that had undergone directed differentiation into early neural (day 7) and differentiated astrocytes (day 21). The heat map for day 7 of differentiation clearly demonstrates differences in expression patterns for each of the lines, with the heterozygous and homozygous null cells clustering more closely (Fig. 5). It is evident that genes associated with cellular function, *Mdk* (Supplementary Fig.

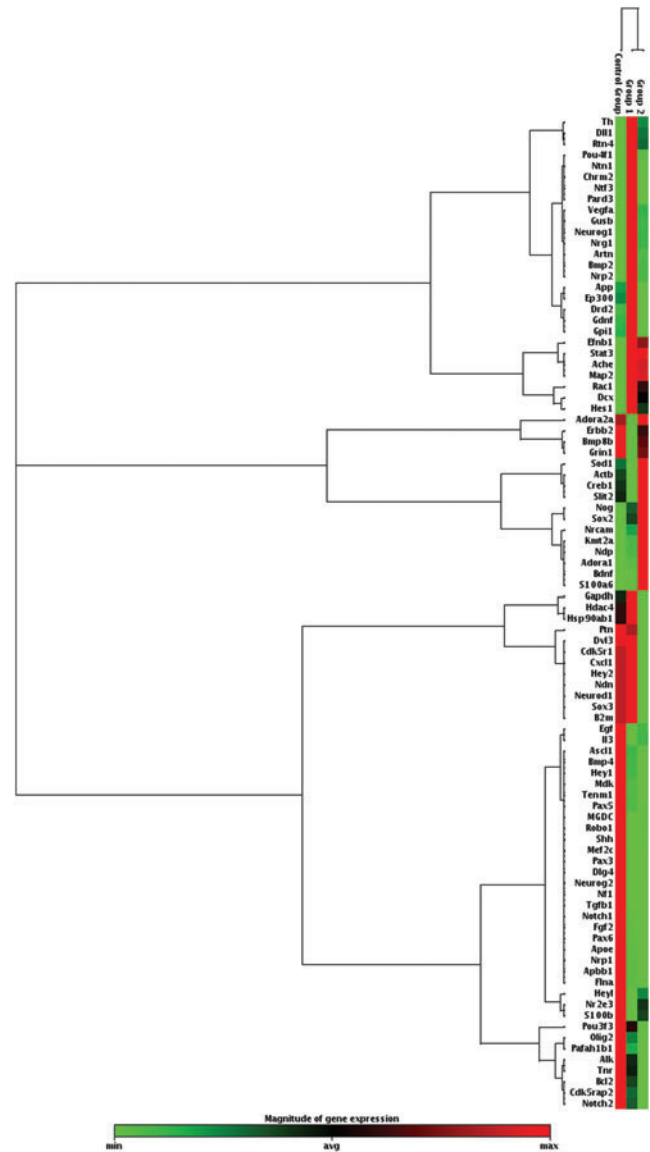


FIG. 5. Heat map of gene expression and clustering from a neuron-specific lineage array performed on ES cells having undergone 21 days of directed neural differentiation. A total of 80 genes from neural lineages were analyzed. Control is wild type, group 1 is +/-, and group 2 is -/-. Color images available online at www.liebertpub.com/scd

S6A and Supplementary Table S8), *Bmp4*, *Il3*, and *Tgfb1* (Supplementary Fig. S6B and Supplementary Table S8), *ApoE* and *S100b* (Supplementary Fig. S6C and Supplementary Table S8), *Efnb1*, *Nrp1*, and *Robo1* (Supplementary Fig. S6D and Supplementary Table S8), and *Apbb1* (Supplementary Fig. S6E and Supplementary Table S8), were significantly downregulated in the heterozygous and homozygous cells. Similar patterns of downregulation of gene expression in the heterozygous and homozygous cells were observed for genes associated with transcriptional regulation (*Ascl1*, *Flna*, *Hey1*, *Neurog2*, *Pax5*, *Pax6*, and *Pou3f3*; Supplementary Fig. S7), neural differentiation pathways (*Oligo2*, *Nrg1*, and *Odz1*; Supplementary Fig. S8), neural signaling pathways (*Shh*; Supplementary Fig. S9), and

synaptic transmission (*Nf1* and *Dlg4*; Supplementary Fig. S10). Notable increases in gene expression for the heterozygous cells were identified in *Artn*, *Nrg1*, *Ntn1*, and *Vegfa* (Supplementary Fig. S6), *Hes1*, *Pax3*, and *Pou4f1* (Supplementary Fig. S7), *Drd2*, *Ntf3*, and *Nrg1* (Supplementary Fig. S8), and *Th* (Supplementary Fig. S10). Likewise, there was a significant increase in homozygous-only cells for just *S100a6* and *Nrcam* (Supplementary Fig. S6). However, gene expression was significantly upregulated in both heterozygous and homozygous null cells for *Neurog1*, *Sox2*, and *Stat3* (Supplementary Fig. S7), *Dcx* (Supplementary Fig. S8), and *DIII* (Supplementary Fig. S9 and Supplementary Table S8). Again, lineage-specific differentiation highlights the effects of disturbed Complex I activity on a cell's differentiation potential.

After 7 days of differentiation, cells from each of the lines were induced to undergo lineage-specific differentiation for a further 14 days. Gene expression patterns revealed that the heterozygous line had threefold higher levels of expression of the early neural marker, *Musashi1* ($P < 0.001$; Fig. 6A). However, the early progenitor markers *Pax6*, *Sox1*, *Ncam*, and *Nestin* had very low levels of expression in the homozygous null line ($P < 0.001$), while in the heterozygous cells, *Ncam* and *Nestin* were expressed at ~50% of the levels for the wild-type cells ($P < 0.001$). Furthermore, the astrocyte endpoint marker, *Gfap*, was expressed at significantly lower levels in the heterozygous and homozygous null cells ($P < 0.001$). We further analyzed the neural endpoint markers, *βIII-tubulin*, *Synaptophysin*, and *Map2*, to determine if there were lineage-specific biases. They were expressed at similar

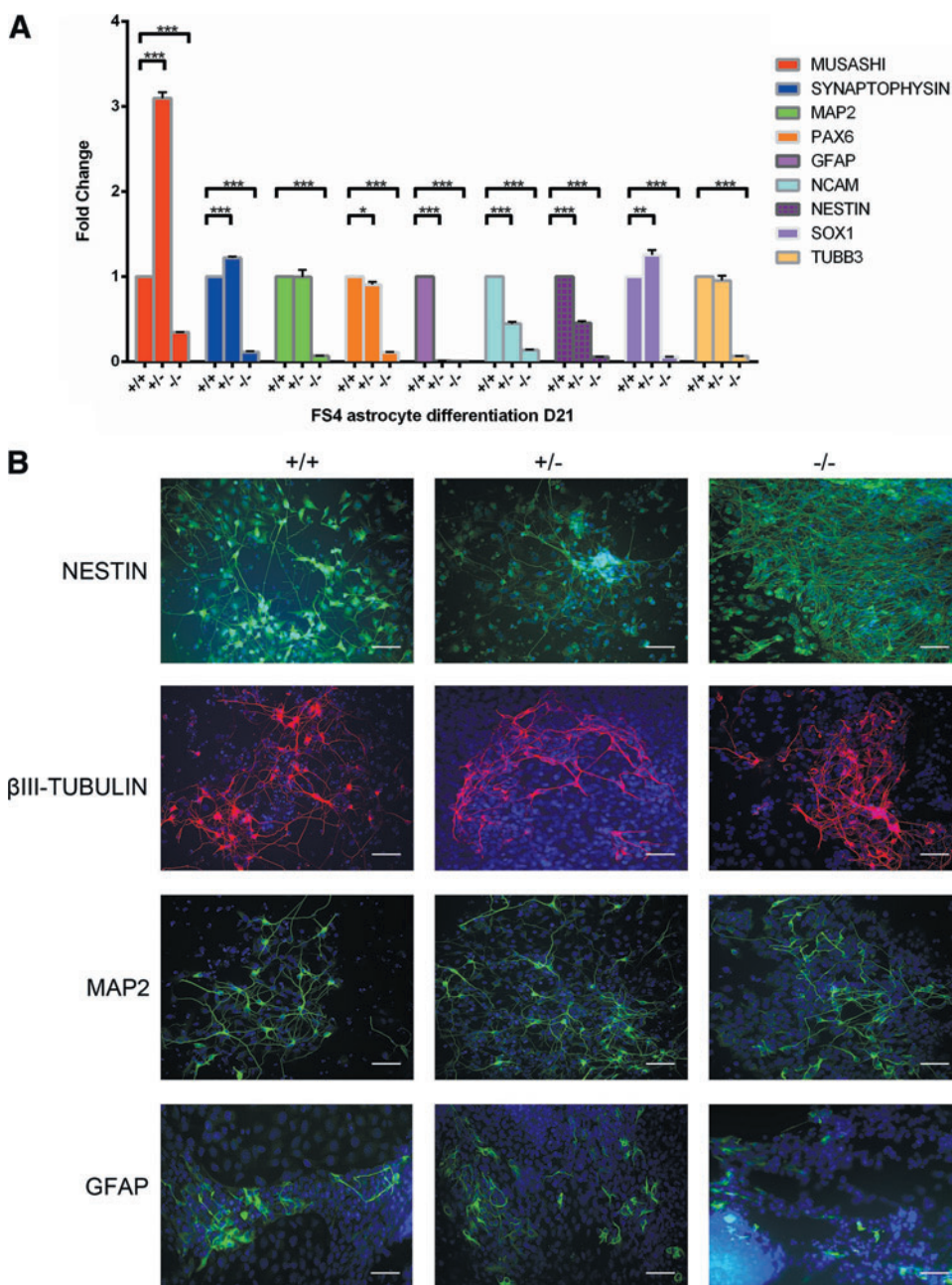


FIG. 6. Analysis of neural gene expression on day 21 differentiated ES cells. ES cells underwent directed differentiation into neural lineages and at day 7 were induced to astrocyte differentiation. **(A)** RT-PCR analysis values represent mean \pm SEM; * $P < 0.05$; ** $P < 0.01$; *** $P < 0.001$. **(B)** Expression in day 21 differentiated ES cells of neuron-specific markers: NESTIN (green), β III-TUBULIN (red), MAP2 (green), and GFAP (green), as determined by immunocytochemistry. Nuclei were stained with DAPI (blue). Scale bar = 50 μ m; magnification = 20 \times . Color images available online at www.liebertpub.com/scd

levels in the wild-type and heterozygous cells but at significantly lower levels in the homozygous null cells ($P < 0.001$). We used immunocytochemistry to confirm that each of the cell lines was able to express the neuron-specific markers, NESTIN, β III-TUBULIN, MAP2, and GFAP (Fig. 6B). Interestingly, mtDNA copy number profiles were very different for each of the lines during differentiation, with the homozygous null line failing to increase mtDNA copy number, exhibiting a significant reduction at day 21 of differentiation ($P < 0.001$; Supplementary Fig. S11).

Complex I enzyme activity was measured on days 18 and 25 of spontaneous differentiation and days 7, 14, and 21 of directed neurogenesis (Table 1). Complex I in the homozygous null cell lines was consistently lower than that in wild-type cells at all stages of differentiation ($P < 0.01$), with estimates ranging from 39% to 75% of the wild-type value. These residual activities are somewhat higher than those found in mouse tissues (10%–22% of wild type in the brain, heart, muscle, liver, and kidney) [11] and mouse cell lines (21%–42% in MEFs, neurons, and astrocytes) [35]. As reported previously, it is technically challenging to distinguish heterozygote from wild-type Complex I enzyme activities [11], but comparison across all differentiation conditions showed Complex I in heterozygotes was lower than wild-type ($P < 0.05$) and higher than homozygous null cells ($P < 0.05$; Table 1).

Discussion

By deriving ES cell lines from a strain of mouse that is notoriously difficult from which to establish ES cell lines [36], we have demonstrated that the deletion of the *Ndufs4* gene induces significant differences to gene expression patterns during early differentiation, which persist at later stages of differentiation. Although mouse ES lines can exhibit chromosomal instability [37,38], each of the *Ndufs4* lines exhibited remarkably normal levels of chromosomal genome stability, except for the one wild-type line exhibiting a CNV. Furthermore, for the mitochondrial genome, only low-level variants were detected, with only one nonsynonymous variant specific to the homozygous null ES cells, present only at a later passage. Although there were differences between the lines for mtDNA copy number and O_2 consumption rates in pluripotent cells, there were no significant differences in total cellular ATP content and lactate levels between each of the lines. Indeed, it is highly likely that each of these lines is primarily dependent on glycolysis at this stage of development, as previously demonstrated for undifferentiated ES cells [19,22,39]. Consequently, the differences in gene expression levels appear to be specific to the deletion of the *Ndufs4* gene.

Cell models of mitochondrial disease have often focused on the use of terminally differentiated cells or cybrids generated by the fusion of an enucleated somatic cell, harboring an mtDNA rearrangement, to an mtDNA-depleted somatic cell [40], which is typically a fibroblast [41,42]. Often, one of the fusion partners is a transformed or tumor/cancer cell line [43], where the potential to analyze the effects of the rearrangement are restricted by the epigenetic status of these cells and their inability to differentiate [33]. The use of ES cells harboring rearrangements affecting a key subunit of the ETC enables the study of early changes in gene expression that can manifest as cells differentiate [19]. We show that ES cells carrying a nucleus-encoded OXPHOS defect, on one or

both alleles, have pluripotent potential as they express the key genes of the pluripotent network, namely *Oct4*, *Sox2*, and *Nanog*. Furthermore, they give rise to teratomas in vivo, demonstrating their potential to differentiate into all cell types of the body. Consequently, they are excellent models to study disorders, such as those associated with Complex I defects, and to determine whether they have their origins during early development. This is essential as many mitochondrial disorders, whether through rearrangements to nucleus- or mitochondria-encoded genes, have an onset early in life.

In this study, we show that both heterozygous and homozygous null rearrangements of *Ndufs4* result in significant changes in Complex I enzyme activity and gene expression profiles during differentiation, especially as OXPHOS has a significant role to play in this process [22]. Perhaps most pertinent is the effect that these rearrangements have on cells that are likely to be dependent on OXPHOS to generate sufficient energy to meet their functional requirements. For example, the homozygous null line exhibited significantly reduced gene expression at late stages in cells induced to undergo astrocyte differentiation, while both the heterozygous and homozygous null cells showed precocious upregulation of neural gene expression in earlier stage cells. Indeed, astrocytes are the most prevalent cell in the brain and have multiple functions. They provide biochemical support for endothelial cells that interact to establish the blood–brain barrier and supply nutrients to neurons, maintain extracellular ion balance, regulate intracellular Ca^{2+} waves, and release transmitters, including glutamate in a Ca^{2+} -dependent manner [44]. Consequently, disruption to any of these processes during early development would have significant implications for neural function and may account for many of the neurological disorders resulting from gene defects associated with OXPHOS. Indeed, gliosis is a common feature in Leigh syndrome and has been observed in one of the *Ndufs4*^{-/-} mouse models [16].

In addition, we determined that there are differences in the ability of *Ndufs4* cells to form beating EBs. The initiation of cardiogenesis is dependent on a hypoxic environment [45], where there would be limited O_2 available to contribute to the synthesis of ATP [46]. Our data show that in an earlier stage of differentiation, there appears to be a greater propensity to form EBs in the homozygous null cells. However, the number of beating EBs reduces at later stages when it is anticipated that there would be more OXPHOS activity in maturing cells to support later stage cardiogenesis. Our analysis of mesodermal gene expression during spontaneous differentiation demonstrated distinct expression patterns for genes associated with cardiogenesis. While expression of *Hand1*, which plays an essential role in early cardiac morphogenesis [47], is similar for the wild-type and homozygous null lines, another regulator of cardiac morphogenesis, *Mixl* [48], is highly overexpressed in the heterozygous and homozygous null cells. Furthermore, *Nppa* and *Ryr2* were highly overexpressed in the mutant lines, and defects to these genes are associated with acute myocardial infarction [49] and mitral valve disease [50], and stress-induced polymorphic ventricular tachycardia and arrhythmogenic right ventricular dysplasia [51], respectively. Similarly, there is a tendency for the heterozygous and homozygous null cells to exhibit increased levels of expression of *Ctsk*, which leads to atherosclerosis [52]. Consequently, the aberrant patterns of gene expression exhibited by the heterozygous and homozygous

lines account for their failure to synchronize beating EB formation during differentiation.

In conclusion, we demonstrate that a defect in the *Ndufs4* gene leads to variable gene expression patterns very early on during differentiation. These aberrant patterns of gene expression continue to manifest during differentiation and, as demonstrated by beating EB formation, bias cellular function and development. Similar outcomes are observed for induced astrocyte differentiation. Our data also support the conclusion that the defects observed are directly influenced by the deletion and not other genetic consequences, namely other chromosomal aberrations or extensive mutation of the mitochondrial genome.

Acknowledgments

We acknowledge Leonie Tutolo from the MCRI for assistance with embryo collection; the facilities and scientific and technical assistance of the Histology Facility, Hudson Institute of Medical Research; and the MHTP Medical Genomics Facility—ACRF Centre for Cancer Genomic Medicine for use of next-generation sequencing and array facilities. This work was supported by the Victorian Government's Operational Infrastructure Support Program; NMHRC Project Grant GNT1022222 to DRT, JCSJ, AEF, SJW, and DRN; an ARC Future Fellowship to MMcK; NHMRC Career Development Fellowships to DRN (GNT1050684) and AEF (GNT541920); and an NHMRC Principal Research Fellowship (GNT 1022896) to DRT.

Author Disclosure Statement

No competing financial interests exist.

References

- Pfeiffer T, S Schuster and S Bonhoeffer. (2001). Cooperation and competition in the evolution of ATP-producing pathways. *Science* 292:504–507.
- Calvo SE and VK Mootha. (2010). The mitochondrial proteome and human disease. *Annu Rev Genomics Hum Genet* 11:25–44.
- Wallace DC and W Fan. (2009). The pathophysiology of mitochondrial disease as modeled in the mouse. *Genes Dev* 23:1714–1736.
- Skladal D, J Halliday and DR Thorburn. (2003). Minimum birth prevalence of mitochondrial respiratory chain disorders in children. *Brain* 126:1905–1912.
- Rahman S and MG Hanna. (2009). Diagnosis and therapy in neuromuscular disorders: diagnosis and new treatments in mitochondrial diseases. *J Neurol Neurosurg Psychiatry* 80:943–953.
- McFarland R, RW Taylor and DM Turnbull. (2007). Mitochondrial disease—its impact, etiology, and pathology. *Curr Top Dev Biol* 77:113–155.
- Lazarou M, M McKenzie, A Ohtake, DR Thorburn and MT Ryan. (2007). Analysis of the assembly profiles for mitochondrial- and nuclear-DNA-encoded subunits into complex I. *Mol Cell Biol* 27:4228–4237.
- McKenzie M, M Lazarou, DR Thorburn and MT Ryan. (2007). Analysis of mitochondrial subunit assembly into respiratory chain complexes using Blue Native polyacrylamide gel electrophoresis. *Anal Biochem* 364:128–137.
- Kirby DM and DR Thorburn. (2008). Approaches to finding the molecular basis of mitochondrial oxidative phosphorylation disorders. *Twin Res Hum Genet* 11:395–411.
- Tucker EJ, AG Compton and DR Thorburn. (2010). Recent advances in the genetics of mitochondrial encephalopathies. *Curr Neurol Neurosci Rep* 10:277–285.
- Leong DW, JC Komen, CA Hewitt, E Arnaud, M McKenzie, B Phipson, M Bahlo, A Laskowski, SA Kinkel, et al. (2012). Proteomic and metabolomic analyses of mitochondrial complex I-deficient mouse model generated by spontaneous B2 short interspersed nuclear element (SINE) insertion into NADH dehydrogenase (ubiquinone) Fe-S protein 4 (*Ndufs4*) gene. *J Biol Chem* 287:20652–20663.
- Leshinsky-Silver E, AS Lebre, L Minai, A Saada, J Steffann, S Cohen, A Rotig, A Munnich, D Lev and T Lerman-Sagie. (2009). *NDUFS4* mutations cause Leigh syndrome with predominant brainstem involvement. *Mol Genet Metab* 97:185–189.
- Petruzzella V, R Vergari, I Puzziferri, D Boffoli, E Lamantea, M Zeviani and S Papa. (2001). A nonsense mutation in the *NDUFS4* gene encoding the 18 kDa (AQDQ) subunit of complex I abolishes assembly and activity of the complex in a patient with Leigh-like syndrome. *Hum Mol Genet* 10:529–535.
- Rahman S, RB Blok, HH Dahl, DM Danks, DM Kirby, CW Chow, J Christodoulou and DR Thorburn. (1996). Leigh syndrome: clinical features and biochemical and DNA abnormalities. *Ann Neurol* 39:343–351.
- Breuer ME, PH Willems, JA Smeitink, WJ Koopman and M Nooteboom. (2013). Cellular and animal models for mitochondrial complex I deficiency: a focus on the *NDUFS4* subunit. *IUBMB Life* 65:202–208.
- Quintana A, SE Kruse, RP Kapur, E Sanz and RD Palmiter. (2010). Complex I deficiency due to loss of *Ndufs4* in the brain results in progressive encephalopathy resembling Leigh syndrome. *Proc Natl Acad Sci U S A* 107:10996–11001.
- Kruse SE, WC Watt, DJ Marcinek, RP Kapur, KA Schenkman and RD Palmiter. (2008). Mice with mitochondrial complex I deficiency develop a fatal encephalomyopathy. *Cell Metab* 7:312–320.
- Ingraham CA, LS Burwell, J Skalska, PS Brookes, RL Howell, SS Sheu and CA Pinkert. (2009). *NDUFS4*: creation of a mouse model mimicking a complex I disorder. *Mitochondrion* 9:204–210.
- Kelly RD, AE Rodda, A Dickinson, A Mahmud, CM Nefzger, W Lee, JS Forsythe, JM Polo, IA Trounce, et al. (2013). Mitochondrial DNA haplotypes define gene expression patterns in pluripotent and differentiating embryonic stem cells. *Stem Cells* 31:703–716.
- Evans MJ and MH Kaufman. (1981). Establishment in culture of pluripotential cells from mouse embryos. *Nature* 292:154–156.
- Chen L and GQ Daley. (2008). Molecular basis of pluripotency. *Hum Mol Genet* 17:R23–R27.
- Ito K and T Suda. (2014). Metabolic requirements for the maintenance of self-renewing stem cells. *Nat Rev Mol Cell Biol* 15:243–256.
- St John J. (2014). The control of mtDNA replication during differentiation and development. *Biochim Biophys Acta* 1840:1345–1354.
- Facucho-Oliveira JM, J Alderson, EC Spikings, S Egginton and JC St John. (2007). Mitochondrial DNA replication during differentiation of murine embryonic stem cells. *J Cell Sci* 120:4025–4034.

25. Facucho-Oliveira JM and JC St John. (2009). The relationship between pluripotency and mitochondrial DNA proliferation during early embryo development and embryonic stem cell differentiation. *Stem Cell Rev* 5:140–158.
26. Kelly RD, A Mahmud, M McKenzie, IA Trounce and JC St John. (2012). Mitochondrial DNA copy number is regulated in a tissue specific manner by DNA methylation of the nuclear-encoded DNA polymerase gamma A. *Nucleic Acids Res* 40:10124–10138.
27. Nagy A, M Gertsenstein, V Kristina and R Behringer. (2003). *Manipulating the Mouse Embryo: A Laboratory Manual*, 3rd edn. Cold Spring Harbor Laboratory Press, Cold Spring Harbor, NY.
28. McKenzie M, M Lazarou and MT Ryan. (2009). Chapter 18 analysis of respiratory chain complex assembly with radiolabeled nuclear- and mitochondrial-encoded subunits. *Methods Enzymol* 456:321–339.
29. Frazier AE and DR Thorburn. (2012). Biochemical analyses of the electron transport chain complexes by spectrophotometry. *Methods Mol Biol* 837:49–62.
30. Sobinoff AP, JM Sutherland, EL Beckett, SJ Stanger, R Johnson, AG Jarnicki, A McCluskey, JC St John, PM Hansbro and EA McLaughlin. (2014). Damaging legacy: maternal cigarette smoking has long-term consequences for male offspring fertility. *Hum Reprod* 29:2719–2735.
31. Yeung KY, A Dickinson, JF Donoghue, G Polekhina, SJ White, DK Grammatopoulos, M McKenzie, TG Johns and JC John. (2014). The identification of mitochondrial DNA variants in glioblastoma multiforme. *Acta Neuropathol Commun* 2:1.
32. Johnston AJ, J Hoogenraad, DA Dougan, KN Truscott, M Yano, M Mori, NJ Hoogenraad and MT Ryan. (2002). Insertion and assembly of human tom7 into the preprotein translocase complex of the outer mitochondrial membrane. *J Biol Chem* 277:42197–42204.
33. Dickinson A, KY Yeung, J Donoghue, MJ Baker, RD Kelly, M McKenzie, TG Johns and JC St John. (2013). The regulation of mitochondrial DNA copy number in glioblastoma cells. *Cell Death Differ* 20:1644–1653.
34. Davis RL, C Liang, F Edema-Hildebrand, C Riley, M Needham and CM Sue. (2013). Fibroblast growth factor 21 is a sensitive biomarker of mitochondrial disease. *Neurology* 81:1819–1826.
35. Bird MJ, XW Wijeyeratne, JC Komen, A Laskowski, MT Ryan, DR Thorburn and AE Frazier. (2014). Neuronal and astrocyte dysfunction diverges from embryonic fibroblasts in the *Ndufs4^{fky/fky}* mouse. *Biosci Rep* 34:e00151.
36. Kawase E, H Suemori, N Takahashi, K Okazaki, K Hashimoto and N Nakatsuji. (1994). Strain difference in establishment of mouse embryonic stem (ES) cell lines. *Int J Dev Biol* 38:385–390.
37. Gaztelumendi N and C Nogues. (2014). Chromosome instability in mouse embryonic stem cells. *Sci Rep* 4:5324.
38. Sanchez-Partida LG, RD Kelly, H Sumer, CY Lo, R Aharon, MK Holland, MK O'Bryan and JC St John. (2011). The generation of live offspring from vitrified oocytes. *PLoS One* 6:e21597.
39. Kelly RD, H Sumer, M McKenzie, J Facucho-Oliveira, IA Trounce, PJ Verma and JC St John. (2013). The effects of nuclear reprogramming on mitochondrial DNA replication. *Stem Cell Rev* 9:1–15.
40. King MP and G Attardi. (1989). Human cells lacking mtDNA: repopulation with exogenous mitochondria by complementation. *Science* 246:500–503.
41. Distelmaier F, WJ Koopman, LP van den Heuvel, RJ Rodenburg, E Mayatepek, PH Willems and JA Smeitink. (2009). Mitochondrial complex I deficiency: from organelle dysfunction to clinical disease. *Brain* 132:833–842.
42. Kirby DM, M Crawford, MA Cleary, HH Dahl, X Dennett and DR Thorburn. (1999). Respiratory chain complex I deficiency: an underdiagnosed energy generation disorder. *Neurology* 52:1255–1264.
43. Hao H, LE Morrison and CT Moraes. (1999). Suppression of a mitochondrial tRNA gene mutation phenotype associated with changes in the nuclear background. *Hum Mol Genet* 8:1117–1124.
44. Agulhon C, J Petravic, AB McMullen, EJ Sweger, SK Minton, SR Taves, KB Casper, TA Fiacco and KD McCarthy. (2008). What is the role of astrocyte calcium in neurophysiology? *Neuron* 59:932–946.
45. Patterson AJ and L Zhang. (2010). Hypoxia and fetal heart development. *Curr Mol Med* 10:653–666.
46. Spitkovsky D, P Sasse, E Kolossov, C Bottinger, BK Fleischmann, J Hescheler and RJ Wiesner. (2004). Activity of complex III of the mitochondrial electron transport chain is essential for early heart muscle cell differentiation. *FASEB J* 18:1300–1302.
47. Riley P, L Anson-Cartwright and JC Cross. (1998). The Hand1 bHLH transcription factor is essential for placenta and cardiac morphogenesis. *Nat Genet* 18:271–275.
48. Hart AH, L Hartley, K Sourris, ES Stadler, R Li, EG Stanley, PP Tam, AG Elefanty and L Robb. (2002). Mixl1 is required for axial mesendoderm morphogenesis and patterning in the murine embryo. *Development* 129:3597–3608.
49. Kim JH, BH Jang, HY Go, S Park, YC Shin, SH Kim and SG Ko. (2012). Potential association between frequent non-synonymous variant of NPPA and cardioembolic stroke. *DNA Cell Biol* 31:993–1000.
50. Curello S, C Ceconi, F De Giuli, A Cargnoni, O Alfieri, A Pardini, P Marzollo, R Mastroiero and R Ferrari. (1991). Time course of human atrial natriuretic factor release during cardiopulmonary bypass in mitral valve and coronary artery diseased patients. *Eur J Cardiothorac Surg* 5:205–210.
51. Lanner JT. (2012). Ryanodine receptor physiology and its role in disease. *Adv Exp Med Biol* 740:217–234.
52. Novinec M and B Lenarcic. (2013). Cathepsin K: a unique collagenolytic cysteine peptidase. *Biol Chem* 394:1163–1179.

Address correspondence to:
Prof. Justin C. St. John
Centre for Genetic Diseases
Hudson Institute of Medical Research
27-31 Wright Street
Clayton, VIC 3168
Australia

E-mail: justin.stjohn@hudson.org.au

Received for publication June 19, 2015
 Accepted after revision November 25, 2015

Prepublished on Liebert Instant Online November 26, 2015